ISSN No: -2456-2165 https://doi.org/10.38124/ijisrt/26may396

Effect of Stator Ovality on Electromagnetic Excitation and Acoustic Noise in a 10-Pole 12-Slot Permanent Magnet Synchronous Motor

Anand Mathiyalagan[1]; Mahesh Babu[2]; Thulasirajan[3]

[1,2,3]R&D EV Motors, Sona BLW Forgings, Chennai, India

Publication Date: 2026/05/29

Abstract: This study investigates the electromagnetic noise and vibration characteristics of a ten-pole, twelve-slot Permanent Magnet Synchronous Motor (PMSM), with particular attention to the influence of stator ovalization. In this topology, the inherent two-lobe structural modes strongly interact with the dominant electromagnetic spatial force harmonic of space order two. This harmonic originates from the fundamental electromagnetic excitation caused by the rotor permanent magnets and slotting and cannot be eliminated through design modifications, making the interaction unavoidable. A simulation-driven workflow was developed to quantify these effects. Electromagnetic analyses were carried out in Dassault Manatee under open-circuit conditions, and the resulting radial and tangential Maxwell stresses were mapped onto the stator inner-tooth surface. These stresses were subsequently coupled with detailed modal parameters extracted from ANSYS to predict vibration velocity and sound pressure levels. Results show that stator ovality significantly amplifies the space-order-two force component, leading to higher modal participation of the two-lobe deformation mode and resulting in increased noise radiation. The proposed workflow provides a reliable approach for predicting electromagnetic NVH behaviour across various deformation scenarios without requiring physical testing.

Keywords: *e-NVH, Electromagnetic forces, PMSM, Stator ovalization, Vibration analysis, Manatee, ANSYS.*

How to Cite: Anand Mathiyalagan; Mahesh Babu; Thulasirajan (2026) Effect of Stator Ovality on Electromagnetic Excitation and Acoustic Noise in a 10-Pole 12-Slot Permanent Magnet Synchronous Motor. *International Journal of Innovative Science and Research Technology*, 11(5), 2199-2208. https://doi.org/10.38124/ijisrt/26may396

I. INTRODUCTION

Electromagnetic noise and vibration (EMNV) in Permanent Magnet Synchronous Motors (PMSMs) have become major design challenges in electric vehicle (EV) applications, where acoustic comfort and structural reliability are critical performance metrics. The primary sources of these excitations are the radial and tangential electromagnetic forces acting on the stator teeth, which arise from permanent magnet fields, slotting effects, and the inherent interaction between stator and rotor magnetic fields. Numerous studies have shown that the slot–pole combination plays a decisive role in shaping the spatial force harmonics and their resulting acoustic signatures [1].

In practical applications, additional geometric or magnetic imbalances frequently arise due to manufacturing tolerances, assembly stresses, or operational factors. Among these, stator ovalization and rotor eccentricity are the most influential, as they distort the air-gap magnetic field and significantly amplify electromagnetic force harmonics. Stator ovality alters the spatial distribution of air-gap permeance and enhances low-order force components that directly excite structural resonance modes. As a result, even a small degree of ovalization can cause a substantial increase in noise levels, especially in EV traction motors where lightweight stator housings and tight NVH requirements intensify the sensitivity to such imperfections.

The PMSM configuration studied in this work is a 10-pole, 12-slot (10P12S) topology, which is widely adopted in automotive traction systems due to its high torque density, reduced torque ripple, and favourable electromagnetic performance. Prior NVH-focused studies have highlighted that although this topology offers lower cogging torque because of its higher least common multiple (LCM), it simultaneously exhibits higher sensitivity to electromagnetic noise due to its non-symmetrical magnetic field distribution (GCD = 2) [1]. This leads to a strong excitation of the space-order-two electromagnetic force harmonic, which naturally couples with the stator's two-lobe deformation mode. Since this harmonic originates from the fundamental magnetic field distribution, its presence cannot be eliminated through conventional design modifications, making the topology inherently susceptible to noise amplification when structural imperfections such as ovalization are present.

Despite the increasing importance of noise in traction motors, limited research has systematically quantified the influence of stator ovalization on electromagnetic force

ISSN No: -2456-2165 https://doi.org/10.38124/ijisrt/26may396

generation and acoustic response for the 10P12S PMSM topology. Existing works [2] have primarily focused on ideal geometries, load conditions, or slot/pole variations, leaving a clear need for a detailed exploration of how manufacturing-induced geometric deviations modify the EM–structural coupling mechanism.

II. THEORETICAL FOUNDATIONS

➢ *Electromagnetic Force Genearation and Force Harmonics*

In PMSMs, the airgap magnetomotive force (MMF) is produced by the combined effect of the rotor permanent magnets and the stator currents. The resulting air-gap flux density can be expressed using an effective permeance formulation, which is commonly adopted for electromagnetic noise analysis [3]. The air-gap flux density is written as

$$B(\theta,t) = \Lambda(\theta)\, F(\theta,t) \quad (1)$$

For a uniform air gap g_0, the permeance is given by $\Lambda_0 = \mu_0/g_0$. Considering the dominant harmonic of the MMF,

$$F(\theta,t) = F_1 cos(p\theta - \omega t) \quad (2)$$

For a 10-pole machine $(p = 5)$, the fundamental airgap MMF is

$$F(\alpha,t) = F_1 cos(5\alpha - \omega t) \quad (3)$$

The corresponding air-gap flux density becomes

$$B(\theta,t) = \frac{\mu_0}{g_0} F_1\, cos(p\theta - \omega t) \quad (4)$$

The electromagnetic forces acting on the stator inner surface are computed using the Maxwell Stress Tensor (MST) formulation [4]:

$$T = \frac{1}{\mu_0}\left(BB - \frac{1}{2}B^2 I\right) \quad (5)$$

From the MST, the radial and tangential electromagnetic force densities along the air gap are expressed as [4, 5]

$$f_r(\theta,t) = \frac{1}{2\mu_0}(B_r^2 - B_t^2) \quad (6)$$

$$f_t(\theta,t) = \frac{1}{\mu_0} B_r B_t \quad (7)$$

These expressions indicate that electromagnetic forces scale with the square of the air-gap flux density. Substituting the fundamental flux density component shows that the dominant dynamic electromagnetic force occurs at spatial order $2p$ and temporal frequency $2f_e$. This force component typically dominates the NVH excitation spectrum in PMSMs [5].

Furthermore, for the studied stator slot and rotor pole combination, harmonic order 2 is identified as the worst-case excitation scenario according to established slot–pole interaction theory [2], since the dominant spatial force order is given by $Z_s - 2p$. For the present machine, $Z_s = 12$ and $2p = 10$, resulting in a harmonic order of $12 - 10 = 2$.

When this force harmonic aligns with the two-lobe stator oval deformation mode, resonance conditions are satisfied, which significantly worsen the radiated noise level. This ovality-induced noise contribution is predominantly observed at $2f_e$and $4f_e$.

In Manatee, rotor–rotor harmonic interactions under open-load conditions are evaluated based on the MMF and permeance orders, and the corresponding force harmonics are computed accordingly. A summary of the dominant MMF orders, permeance orders, and resulting force harmonics is provided in Table 1.0. This table corresponds to rotor–rotor harmonic interactions. Additionally, a magnetic force signature analysis graph is presented in Figure 1, which shows the harmonic spatial order as a function of frequency and rpm. Based on the calculations, the most dominant orders are 0 and 2, which are highlighted in Figure 2.

Table 1 Rotor – Rotor (Open Circuit) Harmonic Force Order Interaction

Rotor Field Harmonic	Slot / MMF Interaction	Resulting Spatial Order (r)	Force Harmonic (H)	Frequency Relation
Br(H5, r = 5) × Br(H5, r = 5)	Self-interaction (PM × PM)	r = 0	H10	2fe
Br(H5, r = 5) × Br(H15, r = 3)	Slot-modulated PM field	r = 2	**H10**	**2fe**
Br(H5, r = −7) × Br(H5, r = 5)	PM sideband	**r = 2**	**H10**	**2fe**

ISSN No: -2456-2165 https://doi.org/10.38124/ijisrt/26may396

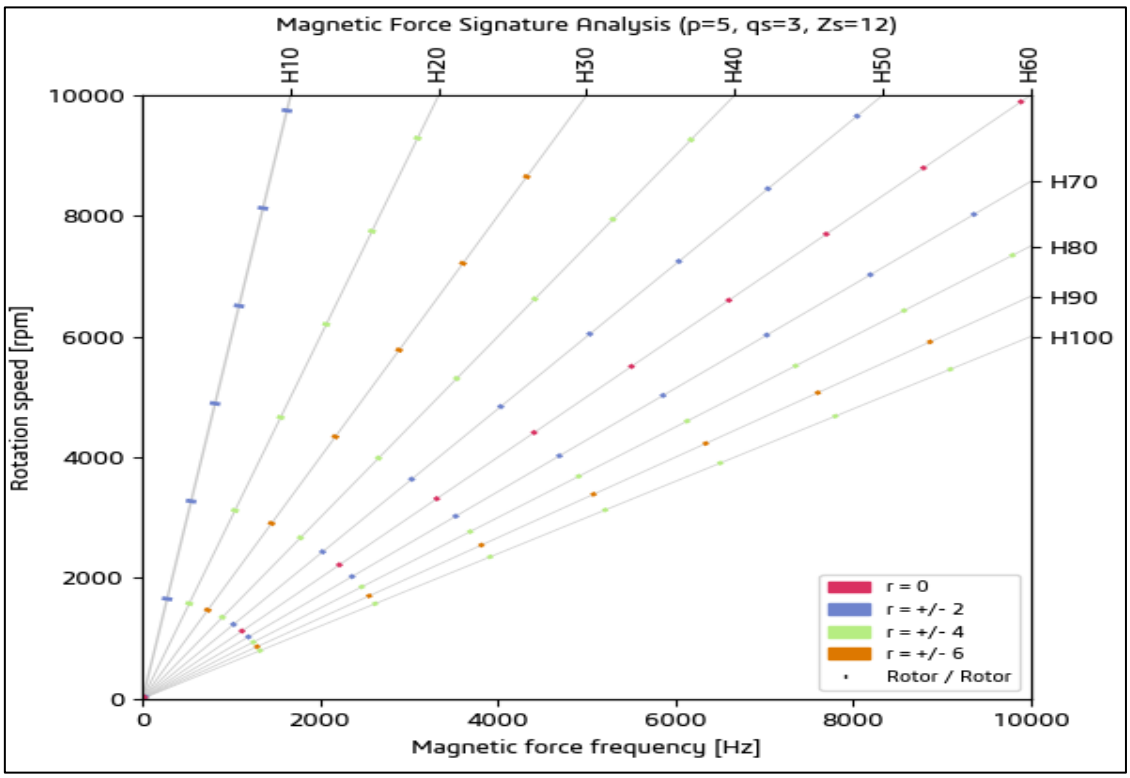

Fig 1 Magnetic Force Signature Analysis of 10p- 12S PMSM

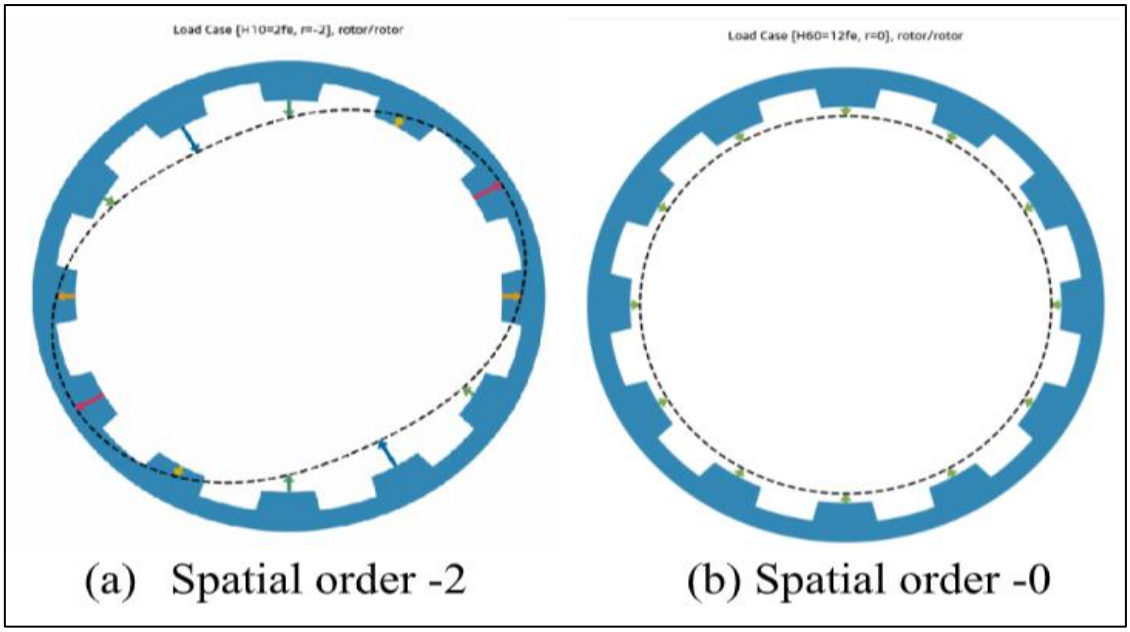

Fig 2 Dominant Spatial Order of 10p- 12S PMSM

In the above table, the dominant electromagnetic force orders corresponding to the given slot–pole combination are summarized. It is evident that the second electrical frequency (2fe) and the second spatial order (r = 2) are critical for this configuration. In addition to the dominant components, three major force-generation mechanisms can be identified.

The first contribution corresponds to the DC component arising from the self-interaction of the fundamental rotor flux harmonic, i.e., H5 × H5. This interaction produces a uniform radial pressure distribution (r = 0) acting equally on all stator teeth. As this pressure does not result in a spatially varying force, it does not effectively excite structural vibration and is therefore not critical for noise radiation in this configuration.

The second contribution originates from the interaction between the fundamental rotor flux harmonic (H5) and the slot-modulated flux harmonic (H15). This interaction generates a force component at H10 (2fe) with a spatial order r = 2, where r = 5 − 3. Here, r = 5 corresponds to the

ISSN No: -2456-2165 https://doi.org/10.38124/ijisrt/26may396

pole-pair order of the rotor field, and r = 3 is induced by the stator slotting effect. This force component is particularly significant due to its low spatial order and strong coupling with structural modes.

The third contribution arises from slot sidebands generated by the modulation of the rotor flux due to stator slotting. These sidebands further interact with the fundamental flux components, producing additional force harmonics at H10 (2fe) with r = 2. As a result, multiple force components coincide at the same frequency and spatial order, leading to a cumulative amplification of the second-order radial force.

Consequently, this slot–pole combination exhibits two dominant second-order excitation mechanisms, both aligned at $2f_e$ and $r = 2$. Such low-order forces are known to efficiently excite two-lobe structural modes, which typically occur at relatively low frequencies and possess high acoustic radiation efficiency. This explains why the present slot–pole combination is particularly unfavorable from an electromagnetic noise and vibration (eNVH) perspective. In addition, the introduced ovality profile generates additional harmonics through its interaction with the permeance variation and flux density. The next chapter discusses how ovality affects the flux distribution and permeance characteristics.

➢ *Flux Density with Ovality*

Using the second-order permeance modulation due to ovality,

$$\Lambda(\alpha) = \Lambda_0[1 - \varepsilon cos(2\alpha + \phi)] \quad (8)$$

The air-gap flux density becomes

$$B(\alpha, t) = \Lambda(\alpha)F(\alpha, t) \quad (9)$$

Substituting (15) and (16):

$$B(\alpha, t) = \Lambda_0 F_1 cos(5\alpha - \omega t) - \varepsilon\Lambda_0 F_1 cos(2\alpha + \phi)cos(5\alpha - \omega t) \quad (10)$$

Applying the product-to-sum identity,

$$cos\, A cos\, B = \frac{1}{2}[cos(A + B) + cos(A - B)] \quad (11)$$

Yields the ovality-induced flux harmonics:

$$B_{ov}(\alpha, t) = -\frac{\varepsilon\Lambda_0 F_1}{2}\Big[cos(7\alpha - \omega t + \phi) + cos(3\alpha - \omega t - \phi)\Big] \quad (12)$$

Stator ovality introduces flux density harmonics of spatial orders 7 and 3 for $p = 5$.

➢ *Electromagnetic Force Generation*

The radial electromagnetic force density is

$$f_r(\alpha, t) = \frac{B^2(\alpha, t)}{2\mu_0} \quad (13)$$

Retaining the dominant cross-product terms between the fundamental and ovality-induced flux components, a second-order spatial force component appears:

$$f_{r,2}(\alpha, t) = F_2 cos(2\alpha - 2\omega t) \quad (14)$$

This term corresponds to a two-lobe standing electromagnetic force.

Decomposition Into CW and CCW Components

Using complex representation,

$$cos(2\theta) = \frac{1}{2}(e^{j2\theta} + e^{-j2\theta}) \quad (15)$$

The force in (22) decomposes into two counter-rotating waves:

$$f_{r,2}(\theta, t) = \frac{F_2}{2}\left(e^{j(2\theta - 2\omega t)} + e^{-j(2\theta - 2\omega t)}\right) \quad (16)$$

Corresponding to clockwise (CW) and counterclockwise (CCW) rotating force components with spatial orders

$$r = \pm 2 \quad (17)$$

For the investigated 10-pole machine ($p = 5$), stator ovality introduces flux density harmonics of orders 3 and 7, whose interaction through Maxwell stress generates a dominant second-order electromagnetic force that strongly couples with the stator two-lobe vibration mode.

➢ *Modal: Analytical Background*

The second objective of the e-NVH simulation is to identify the natural frequencies of the stator and to determine whether these frequencies coincide with the dominant electromagnetic force excitations. Any such coincidence may lead to resonance, which becomes more critical in the presence of stator ovalization, as ovality modifies the stiffness distribution and shifts the natural frequencies. Several studies have investigated the estimation of stator natural frequencies using analytical and numerical approaches [8].

In analytical investigations, the stator is commonly idealized as a thin cylindrical shell, where the integers $m$and $n$represent the longitudinal and circumferential deformation modes, respectively [9]. Lower-order circumferential modes ($n = 0,1,2$) generally exhibit the largest vibration amplitudes, with the $n = 2$mode corresponding to the two-lobe (ovalization) deformation, which is particularly critical for electromagnetic noise.

ISSN No: -2456-2165 https://doi.org/10.38124/ijisrt/26may396

For circumferential modes $i \geq 2$, the equivalent circumferential wave number is expressed as [9]

$$k_i = \frac{\pi}{a}\sqrt{i^2 - 1} \tag{18}$$

Where $a$is the mean stator radius. The corresponding modal stiffness and natural frequency of the cylindrical shell are given by [9],

$$k_{ic} = \frac{EI_c}{M_{md}} k_i^4 \tag{19}$$

$$\omega_i^2 = \frac{k_{ic}}{M_{md} + M_{rot}}\left[1 + \frac{4(k_i a)^2}{i^2 - 1}\right] \tag{20}$$

Where $E$is Young's modulus, $I_c$is the circumferential second moment of area, $M_{md}$is the stator distributed mass, and $M_{rot}$is the equivalent rotating mass contribution. These shell-based equations provide physical insight into the dependence of natural frequencies on geometric and material parameters, particularly for the two-lobe ovalization mode. However, such formulations rely on simplifying assumptions such as uniform thickness and neglect of slotting, windings, and laminated construction.

Therefore, in the present work, the stator modal characteristics are obtained using three-dimensional finite element analysis. The undamped free-vibration behaviour of the stator structure is governed by the multi-degree-of-freedom equation of motion

$$M\ddot{x} + Kx = 0, \tag{21}$$

Where Mand Kdenote the mass and stiffness matrices of the structure, respectively, and x is the physical displacement vector. Solving the corresponding eigenvalue problem

$$(K - \omega^2 M)\phi = 0 \tag{22}$$

Yields the natural frequencies ω_n and corresponding mode shapes $\phi_n$of the stator structure [9], [10]. Low-order circumferential modes, particularly the $(2, 0)$ ovalization mode, are of special interest due to their strong interaction with electromagnetic force harmonics in electrical machines.

- *Harmonic Response Analysis Using Modal Superposition*

The forced vibration response of the stator under electromagnetic excitation is evaluated using the modal superposition (MSUP) method. The governing equation of motion including damping is expressed as

$$M\ddot{x} + C\dot{x} + Kx = F(t), \tag{23}$$

Where Cis the damping matrix and $F(t)$represents the time-varying electromagnetic force vector [11].

The physical displacement vector is expressed in terms of modal coordinates as

$$x(t) = \Phi q(t), \tag{24}$$

Where $\Phi = [\phi_1, \phi_2, \ldots, \phi_N]$ is the modal matrix obtained directly from the preceding modal analysis, and $q(t)$is the vector of generalized modal coordinates [9], [12].

Substituting (32) into (31) and applying modal orthogonality leads to a set of uncoupled modal equations:

$$\ddot{q}_j + 2\zeta_j \omega_j \dot{q}_j + \omega_j^2 q_j = f_{jc}(t), \tag{25}$$

Where ω_j and ζ_j denote the natural frequency and damping ratio of the jth mode, respectively, and $f_{jc}(t)$is the generalized modal force corresponding to that mode [11], [13].

For harmonic electromagnetic excitation at angular frequency Ω, the steady-state modal response is obtained using the dynamic stiffness formulation

$$q_{jc} = \frac{f_{jc}}{(\omega_j^2 - \Omega^2) + j(2\zeta_j \omega_j \Omega)}, \tag{26}$$

Which highlights the resonance condition when the excitation frequency approaches the natural frequency of a structural mode [11], [14].

The total structural response in the physical domain is reconstructed by superposition of the individual modal contributions as

$$x(\Omega) = \sum_{j=1}^{N} \phi_j \, q_{jc}. \tag{27}$$

This frequency-domain formulation enables efficient prediction of resonance phenomena arising from the interaction between electromagnetic force harmonics and stator structural modes, particularly when low-order force harmonics coincide with stator ovalization modes [14].

- *Analytical Basis for Acoustic Radiation Estimation*

The acoustic response of the electric machine was evaluated using the Equivalent Radiated Power (ERP) method, which estimates the radiated acoustic energy directly from the structural vibration results without meshing the air domain [1]. In this approach, each surface node of the structure is treated as a small acoustic radiator, and the total radiated power is computed by summing the contribution of all vibrating nodes, providing an efficient alternative to coupled vibro-acoustic simulations that require significantly higher computation [16]. The ERP value is obtained using

$$ERP = \sum_{i=1}^{N} \frac{1}{2} \rho_0 c_0 A_i v_{n,i}^2 \tag{28}$$

ISSN No: -2456-2165 https://doi.org/10.38124/ijisrt/26may396

Where ρ_0 is the air density, c_0 is the speed of sound, A_i is the elemental area, and $v_{n,i}$ is the normal vibration velocity [15], [16]. To convert vibration into acoustic pressure, the radiating surface is modeled using a classical acoustic monopole representation, which relates the radiated pressure at a distance r to the volume velocity $\dot{V}$ using

$$p(r) = \frac{\rho_0 c_0 \, Q\dot{V}}{4\pi r} \tag{29}$$

Where Q is the directivity coefficient. In this study, $Q = 2$ was selected to represent hemispherical radiation corresponding to a bench-mounted machine [15]. This formulation assumes a homogeneous and infinite acoustic medium—commonly referred to as the free-field assumption—where air density and sound speed are constant, and acoustic pressure decays proportionally to $1/r$. SPL at the microphone is finally reconstructed using the standard relation

$$SPL = 20log_{10}\left(\frac{p(r)}{p_{ref}}\right) \tag{30}$$

With $p_{\text{ref}} = 20\,\mu\text{Pa}$. These combined assumptions allow ERP to provide a computationally efficient yet physically meaningful estimate of the radiated noise from electric machines [15], [16].

III. SIMULATION METHODOLOGY

Before presenting the detailed simulation methodology, an overview of the complete NVH workflow is provided in Figure 3. This high-level flow illustrates the sequence of electromagnetic, structural, and acoustic analyses that form the foundation of the NVH evaluation process.

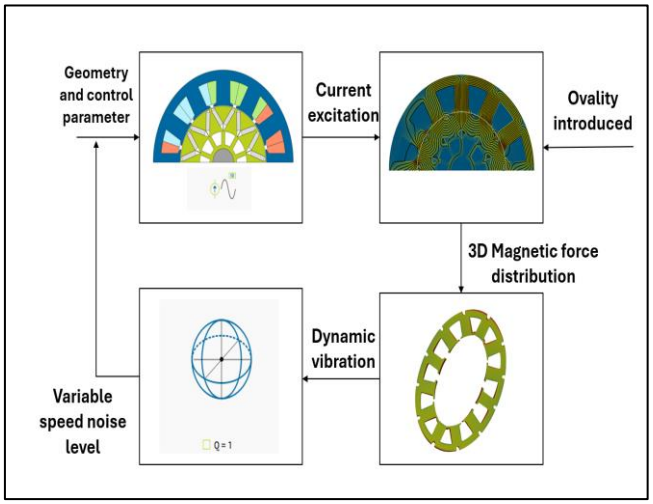

Fig 3 Manatee NVH Workflow

➢ *Two-Dimensional Electromagnetic Analysis*

Electromagnetic simulations were performed using Dassault Systems MANATEE, as schematically shown in Figure 4. The machine under study is a 10-pole, 12-slot (10P–12S) configuration with concentrated windings and a delta connection. The stator magnetic material was modelled using M235-35A electrical steel, and the rotor permanent magnets were defined using N45UH material. A two-step linear skew was applied to reduce torque ripple.

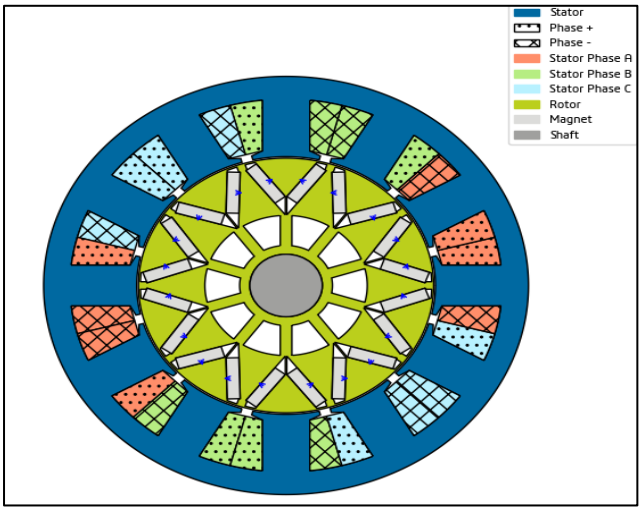

Fig 4 Two-Dimensional Model of a 10-Pole 12-Slot Permanent Magnet Synchronous Motor

Based on the above input configuration, the rotor MMF spatial orders were evaluated and are shown in Figure 5. As expected, the fifth spatial order is dominant and corresponds to the fundamental MMF component. In addition, the third-, fifth-, and seventh-order harmonic components are observed. A detailed explanation of the electromagnetic force generation mechanism and spatial order calculation is provided in the subsequent sections.

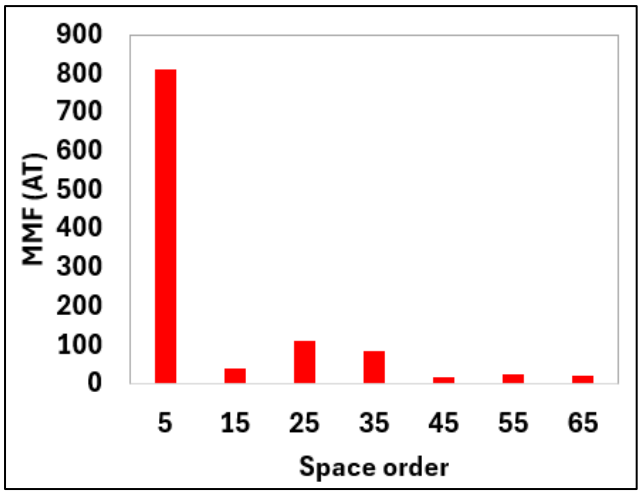

Fig 5 Rotor Magnetomotive Force Order

The air-gap length was set to 0.6 mm, representing the ideal nominal condition. Second-order stator ovality was introduced to study its influence on electromagnetic excitation, as shown in Figure 6.0. The ovality magnitude was varied from 0 to 200 µm in increments of 50 µm, with the deformation applied 180 electrical degrees apart.

ISSN No: -2456-2165 https://doi.org/10.38124/ijisrt/26may396

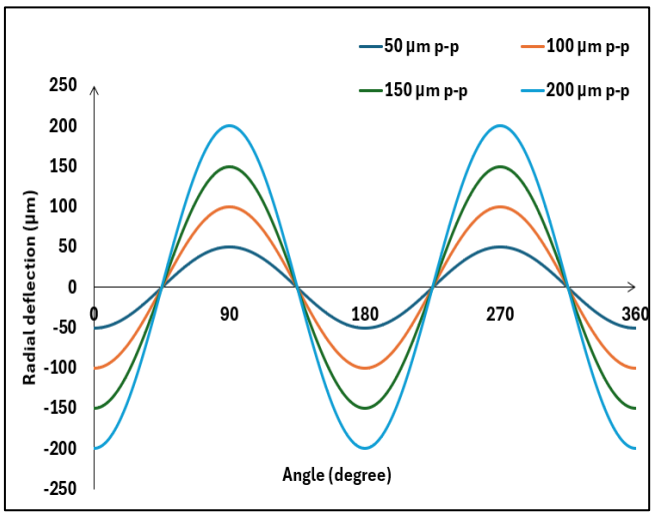

Fig 6 Second Order Stator Air Gap Ovality

➢ *Three-Dimensional Modal & Acoustic Analysis*

A full 3D modal analysis was performed using ANSYS Workbench, including the Motor housing and stator Figure 7 shows the 3D stator model highlighting the dominant NVH-sensitive mode shapes, along with a sectional view of the full assembly.

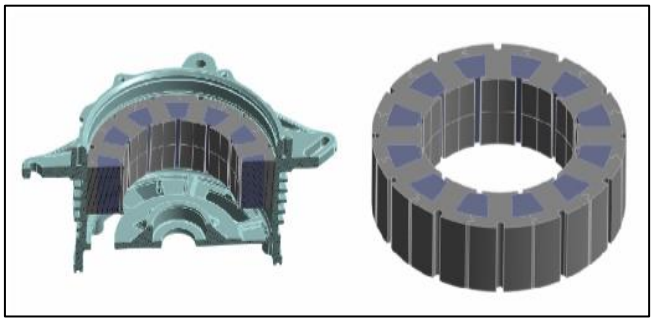
Fig 7 Motor Assembly and Stator Assembly with Simplified Winding

To reduce preprocessing complexity and computational time, the winding geometry was simplified and modelled as a solid block, following the approach described in [4]. Since the analysis is linear dynamic in nature, linear elastic material properties were assigned to all components. The contacts between structural parts were modelled using bonded contact, which is appropriate for linear modal simulations. Orthotropic properties of the stator lamination (M235–35A) were not included because complete characterization data for this material was unavailable.

The modal extraction range was selected up to $4f_e$ (four times the electrical frequency). For a 10P/12S PMSM, the $2f_e$ ovalization mode is the dominant NVH contributor, and stator ovality introduces additional ±2 spatial harmonic interactions, making it essential to capture modes at least up to $4f_e$. For example, at 7500 rpm, $4f_e$ corresponds to approximately 2500 Hz. A preliminary modal run was carried out to verify that all two-lobe structural modes of interest are included within this range. If any critical mode is outside the extracted band, the upper frequency limit and number of extracted modes should be increased accordingly.

The acoustic model employed in this study is based on the Equivalent Radiated Power (ERP) method. The sound pressure level is computed using an equivalent monopole source positioned at the center of a 3D radiating envelope, with the distance from each envelope node to the virtual source considered in the radiation calculation. The physical surface of the machine is not explicitly modeled in this approach. A free-field condition is assumed, and the microphone is placed 1 mm from the machine center. A directivity coefficient of $Q = 2$ is applied, corresponding to a bench-level test configuration, as highlighted in Figure 8.

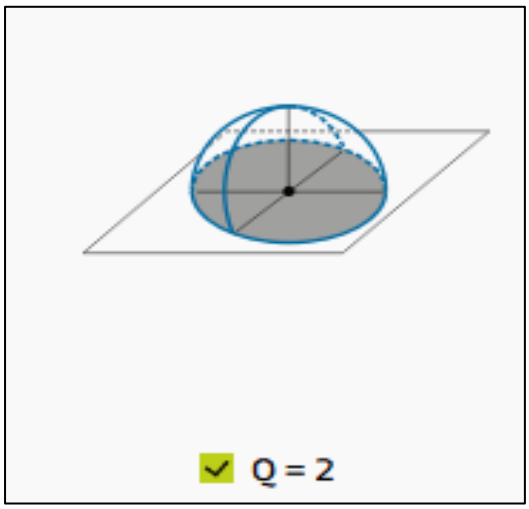

Fig 8 Acoustic Radiator

IV. RESULTS AND INTERPRETATION

Before presenting the results, it is noted that, unless otherwise specified, all results are shown at 6857 rpm, at which the maximum noise is observed. In certain cases, results are also presented in the form of speed (rpm) versus noise plots. Furthermore, all results correspond to the radial force components, as the tangential force component is negligible in the absence of unbalanced magnetic forces [9].

➢ *Flux Harmonics*

The highest flux density is observed at the fundamental electrical frequency corresponding to 6857 rpm (114 Hz × 5 pole pairs), as expected. Consequently, the third-, fifth-, and seventh-order harmonics are also present, consistent with the rotor MMF spatial orders. The flux harmonics are largely independent of stator ovality; however, when combined with the permeance variation, they generate additional harmonic components in the resulting Maxwell force. The influence of ovality becomes significant only when the complete flux density expression is substituted into the Maxwell force equation, as highlighted in (12).

It is further noted that only odd-order harmonics are present, as even-order harmonics are cancelled both mathematically and physically due to the symmetry between the north and south magnetic poles. When stator ovality is considered, the third- and fifth-order spatial harmonics become dominant, as indicated in (12). As the ovality

ISSN No: -2456-2165 https://doi.org/10.38124/ijisrt/26may396

increases, the amplitude of the third-order harmonic increases, whereas the seventh-order harmonic remains largely unchanged as illustrated in Figure 9.

During the electromagnetic force calculation, the interaction between flux density harmonics and permeance variation produces additional force harmonics, particularly at $2f_e$ and $4f_e$. Among these, the $4f_e$ component is especially critical because it can easily interact with structural modes and significantly amplify vibration and acoustic noise.

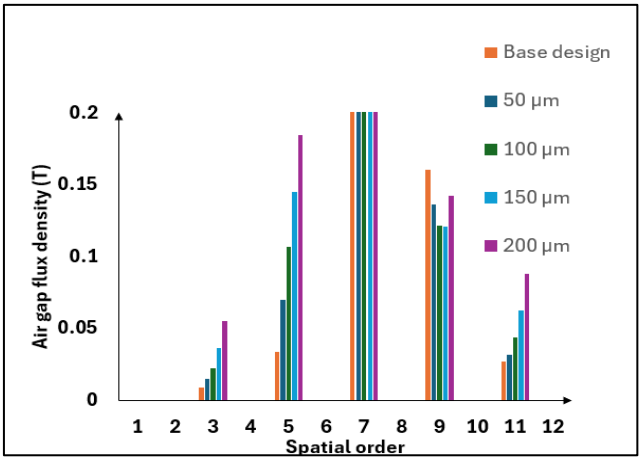

Fig 9 Radial Flux Density and Spatial Order for Different Ovality Conditions.

➢ *Electromagnetic Forces and its Harmonics*

The Maxwell force is decomposed into a single lumped magnetic force component, as described in [10]. In the following plot, the forces are presented as the maximum values over the circumferential angle. As expected, the DC component of the force decreases with increasing air-gap ovality, since the increased effective stator–rotor magnetic distance reduces the average magnetic attraction force.

In contrast, the fundamental harmonic component (H10 – $2f_e$) and the second-order harmonic component (H20 – $4f_e$) increase with increasing ovality. The fundamental component at $2f_e$ cannot be eliminated due to the inherent slot–pole combination and remains significant even in the absence of ovality. This behavior is governed by the dominant spatial order of ± 2, as already indicated in (10). It should be noted that the forces shown here represent the combined contribution of all spatial orders as illustrated in Figure 10.

With respect to the second-order harmonic (H20 – $4f_e$), a strong interaction with stator ovality is observed. This component exhibits negligible force magnitude in the nominal (non-ovality) case; however, with the introduction of ovality, it increases significantly. The coupling between stator ovality and flux density, and the resulting formation of a second-order spatial force pattern, are explained in (33).

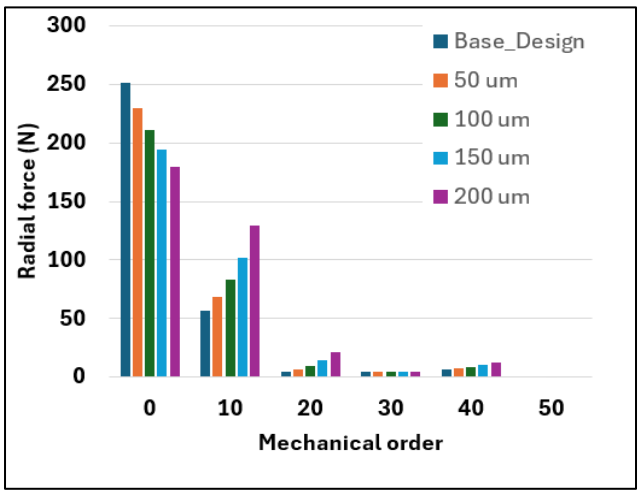

Fig 10 Radial Tooth Lumped Force Harmonic Components at 6857 rpm

➢ *Modal Analysis*

The mode shapes obtained from the free–free modal analysis are shown in Figure 11. As expected, the dominant structural mode is the (2,0) two-lobe mode, observed at 2270 Hz as shown in Figure 11(b). With respect to rotational speed, this mode aligns closely with the H20 mechanical order, which corresponds to the second harmonic of the fundamental electromagnetic excitation (4 f_e). This alignment is the primary reason for the increased noise level, in addition to the contribution from the fundamental component.

The breathing mode (0,0) is also observed as illustrated in Figure 11(a); however, its impact is comparatively lower in this case. This is because the cogging torque order of the machine is H60 (LCM of slots and poles: 10 and 12), as discussed in [1]. This represents a key advantage of the selected slot–pole combination, which is also highlighted in the FRF results. Although the breathing mode exhibits a significant vibration level from a structural standpoint, there is no corresponding electromagnetic spatial order (0,0) to effectively excite this mode.

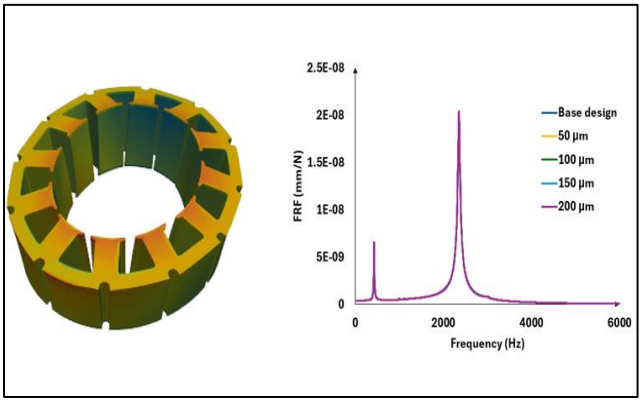

(a) Breathe mode (0,0) – 2340 Hz

ISSN No: -2456-2165 https://doi.org/10.38124/ijisrt/26may396

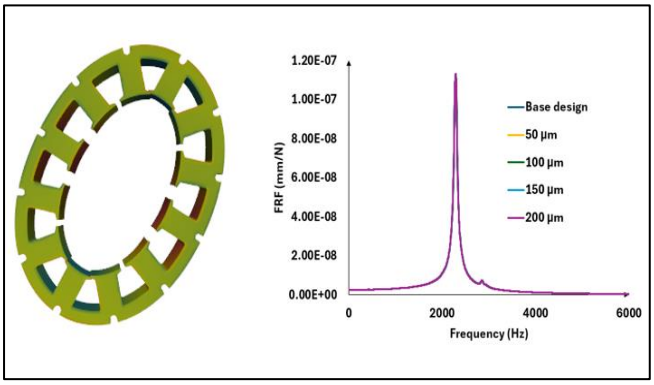

(*b*) Two lobe mode (2,0) – 2270 Hz
Fig 11 Different Mode Shapes of Stator & FRF

➢ *Vibration Velocity Response*

The vibration velocity level is evaluated at the outer radiating surfaces of the motor casing. As the rotational speed increases, the excitation frequencies progressively align with the structural modes of the system. For the H10 component, the maximum 10th-order excitation at 7500 rpm corresponds to 1250 Hz, which is primarily governed by the slot–pole combination. The maximum vibration velocity level of 132 dB is observed at 6857 rpm under a 200 µm ovality condition for the H10 order as shown in Figure 12.

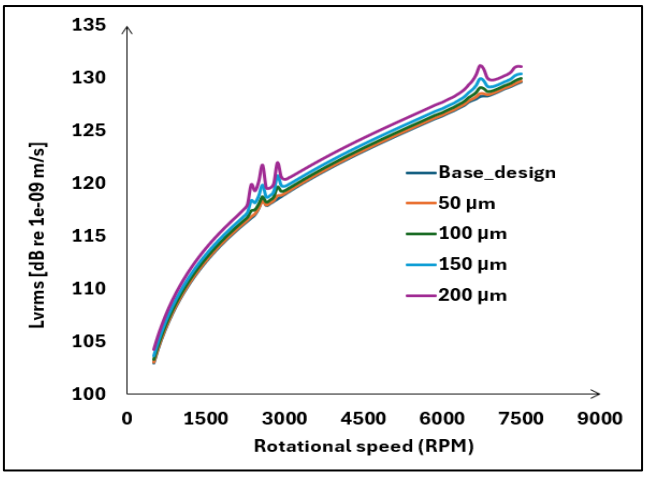

Fig 12 Vibration Velocity at H10 ($2f_e$) as a Function of Rotational Speed.

A secondary harmonic component is observed around 3000 rpm at approximately 50 Hz; when expressed in terms of the 10th order, this corresponds to 500 Hz. Similarly, at 6857 rpm, an excitation at approximately 114 Hz corresponds to 1142 Hz in terms of the 10th order. These frequencies are close to structural natural frequencies and therefore indicate a potential interaction with rotor structural mode shapes. This interaction requires further verification.

For the H20 order, the dominant noise response is observed at 6857 rpm at 2285 Hz, which strongly aligns with a two-lobe structural mode at the same frequency, as shown in Figure 13. In the absence of ovality, the vibration velocity response is primarily driven by the fundamental component, and the H20-related velocity level remains limited to approximately 85 dB. However, with increasing ovality, the vibration velocity associated with the H20 order increases proportionally and reaches approximately 140 dB for the 200 µm ovality case, exceeding the fundamental component. Up to 100 µm ovality, the vibration velocity is mainly driven by the slot–pole-induced fundamental excitation; beyond this level, the response becomes dominated by ovality-induced forces.

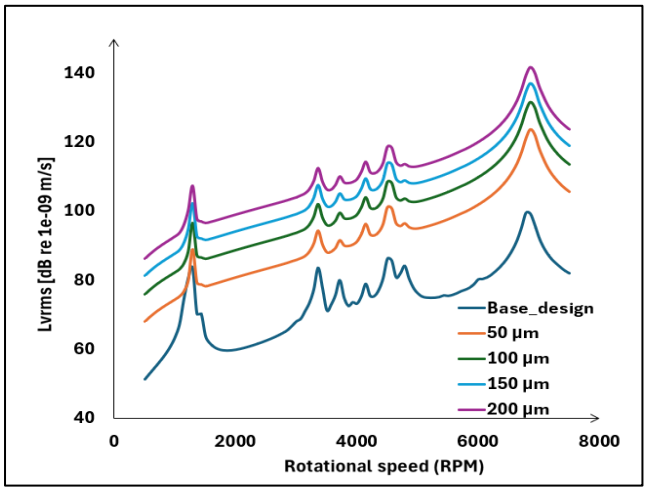

Fig 13 Vibration Velocity at H20 ($4f_e$) as a Function of Rotational Speed.

➢ *Acoustic Results (Sound Pressure Level)*

The sound pressure level is calculated from the vibration velocity using the expressions given in (28)–(30). Since the sound pressure level is directly derived from the vibration velocity, the observed trends closely follow the vibration response discussed previously.

In the absence of ovality, the maximum sound pressure level is approximately 80 dB, with the response dominated by the H10 component. After introducing ovality, no significant change is observed in the H10 component; however, the H20 component gradually increases beyond 100 µm ovality. At higher ovality levels, the H20 component completely dominates the response, leading to a maximum sound pressure level of approximately 90 dB.

V. CONCLSUION

This paper investigates the electromagnetic noise and vibration behavior of a 10-slot–12-pole (10S–12P) machine under different stator ovality conditions. The baseline topology inherently produces a strong $2f_e$ excitation due to its slot–pole combination. The introduction of stator ovality significantly amplifies the noise and vibration response, particularly at the H10 and H20 harmonic orders.

The H10 component is intrinsic to the machine topology and cannot be eliminated through ovality-related design changes. Stator ovality further increases the response at H10 and induces a strong H20 component, for which vibration becomes the dominant contributor to the overall acoustic response. These effects are not unique to the 10S–12P configuration and are expected in machines where the greatest common divisor (GCD) of the slot and pole numbers

ISSN No: -2456-2165 https://doi.org/10.38124/ijisrt/26may396

equals two, leading to critical $2f_e$ excitations. While such configurations are favorable for cogging torque reduction due to a higher least common multiple (LCM), they are unfavorable from an eNVH perspective.

Future work will focus on mitigation strategies, including rotor and stator notching, structural stiffening, and the introduction of damping treatments to suppress vibration and reduce radiated noise. The impact of these measures on electromagnetic performance, particularly torque reduction, will also be assessed.

REFERENCES

[1]. AIP Advances, "AIP Advances 14, 015127 (2024)," AIP Advances, vol. 14, p. 015127, 2024, doi:10.1063/9.0000647.

[2]. Devillers, E., Le Besnerais, J., Souron, Q., and Hecquet, M., "Characterization of acoustic noise and vibrations due to magnetic forces in induction machines for transport applications using MANATEE software," EOMYS Engineering & L2EP, Lille, France, Technical Report, 2012.

[3]. Le Besnerais, J., et al., "Electromagnetic Force Harmonics and Noise in PMSMs," IEEE Transactions on Industry Applications, vol. 48, no. 6, pp. 1869–1877, 2012.

[4]. Boglietti, A., Cavagnino, A., Staton, D., and Popescu, M., "Iron loss in electrical machines: Influencing factors, model, and computation," IEEE Transactions on Magnetics, vol. 44, pp. 3169–3172, 2008.

[5]. Gieras, J. F., Noise of Polyphase Electric Motors, CRC Press, Boca Raton, FL, USA, 2006.

[6]. F. Chai et al., "Accurate modelling and modal analysis of stator systems in PMSMs," IET Electric Power Applications.

[7]. Hecquet, M., Brochet, P., and Vannier, J. C., "Influence of air-gap eccentricity and ovality on electromagnetic noise," IEEE Transactions on Magnetics, vol. 41, no. 5, pp. 1624–1627, May 2005.

[8]. El Khawly, Z., and Schramm, D., "Analytical modal analysis for the stator system of a permanent magnet synchronous motor for hybrid vehicles and calculation of its natural frequencies," Proc. IEEE International Conference on Electrical Machines and Systems (ICEMS), Busan, South Korea, 2013.

[9]. Ewins, D. J., Modal Testing: Theory, Practice and Application, 2nd ed., Research Studies Press, Baldock, U.K., 2000.

[10]. Meirovitch, L., Analytical Methods in Vibrations, Macmillan, New York, NY, USA, 1967.

[11]. Rao, S. S., Mechanical Vibrations, 6th ed., Pearson, Upper Saddle River, NJ, USA, 2017..

[12]. Inman, D. J., Engineering Vibration, 4th ed., Pearson, Upper Saddle River, NJ, USA, 2014.

[13]. Meirovitch, L., Analytical Methods in Vibrations, Macmillan, New York, NY, USA, 1967.

[14]. Géradin, M., and Rixen, D., Mechanical Vibrations: Theory and Application to Structural Dynamics, 3rd ed., Wiley, Hoboken, NJ, USA, 2015.

[15]. Xiong, Q., et al., "Equivalent Radiated Power (ERP) Levels Used in Motor Vibro-Acoustic Analysis," Noise, vol. 1, no. 1, 2025.

[16]. FunctionBay Inc., "What is Equivalent Radiated Power (ERP) which is used in RecurDyn/Acoustics?," FunctionBay Technical FAQ, published Oct. 15, 2019. Accessed 2026. Available: https://functionbay.com/en/faq/single/502/WhatisERP-en